Available online at www.sciencedirect.com
ScienceDirect
Ceramics International 35 (2009) 2295–2304
CERAMICS INTERNATIONAL
www.elsevier.com/locate/ceramint

Nanoindentation study of microplasma sprayed hydroxyapatite coating

A. Dey [a], A.K. Mukhopadhyay [b,*], S. Gangadharan [a], M.K. Sinha [a], D. Basu [a], N.R. Bandyopadhyay [c]

[a] Bio-Ceramics and Coating Division, Central Glass and Ceramic Research Institute, Kolkata 700 032, India
[b] Mechanical Test Section, Analytical Facility Division, Central Glass and Ceramic Research Institute, Kolkata 700 032, India
[c] School of Materials Science and Engineering, Bengal Engineering and Science University, Shibpur, Howrah 711 103, India

Received 1 October 2008; received in revised form 10 November 2008; accepted 7 January 2009
Available online 22 January 2009

Abstract

The microplasma sprayed (MPS) hydroxyapatite (HAP) coating on surgical grade SS316L, is an emerging material for bio-ceramic based implant application involving higher reliability. For this purpose, a 200 μm thick MPS-HAP coating was developed on SS316L substrate and characterized by XRD, SEM and FE-SEM techniques. The local mechanical properties of the coating, e.g. nano-hardness and Young's modulus were evaluated by nanoindentation technique carried out with a Berkovich indenter at various depths in the range of about 170–3000 nm on a polished top surface. The characteristic values of nano-hardness (1.5–5 GPa) and Young's modulus (∼60–100 GPa) obtained through the application of Weibull statistics to the experimentally measured data revealed a strong indentation size effect (ISE). Attempts were made to explain the genesis of ISE on the basis of some existing and some new concepts.

Keywords: A. Films; C. Mechanical properties; C. Hardness; E. Biomedical applications

1. Introduction

Over the past few years, hydroxyapatite (HAP) has been mainly introduced as a porous coating on metallic implants to provide easier in-growth of bony tissues. The excellent biocompatibility and bio-stability of HAP coatings have become well established and the usages of this material for prosthetic applications have been rapidly popularized in the past few years. Plasma spraying (PS) with a high plasmatron power (e.g. 20–40 kW) is the most popular and commercially accepted coating method. However, due to the high temperature of plasma jet, the degradation of HAP was unavoidable during spraying, which involved the formation of undesirable tetracalcium phosphate (TTCP), tricalcium phosphate (TCP) and calcium oxide phases. In addition, due to the rapid cooling of sprayed particles, amorphous calcium phosphate also forms in the HAP coatings on Ti6Al4V substrates [1,2]. The degree of crystallinity (X_c) of PS-HAP coatings usually lied below 70% [3]. The lower the degree of crystallinity, the lower was the stability of the coating in vivo. To tackle these problems, recently the microplasma spraying (MPS) process with a low plasmatron power (e.g. 1–4 kW) has been introduced because it can provide a higher degree of crystallinity, e.g. $X_c \sim 90\%$ and phase purity than those provided by conventional PS [4]. In the present work, the metallic substrate chosen was a surgical grade, biocompatible austenitic stainless steel (SS316L). The choice was prompted by better corrosion resistance properties, mechanical properties and lower cost of SS316L than those of the conventional Ti6Al4V alloy [5–7].

The stability and reliability of the coated implant in vivo depend predominantly upon the local mechanical properties of the coating. In the present work, a low plasmatron power (∼1.5 kW), i.e. microplasma was used to coat HAP on SS316L and the local mechanical properties, e.g. nano-hardness (H) and Young's modulus (E) of the MPS-HAP coating were evaluated by the well established nanoindentation technique. The local mechanical properties, e.g. H and E of HAP and/or HAP composite coating as well as global mechanical properties, e.g. microhardness have not been reported to a great detail in literature. Most of the researchers reported nanoindentation data with a Berkovich indenter for plasma sprayed HAP coating

* Corresponding author. Tel.: +91 33 2473 3469/76/77/96; fax: +91 33 2473 0957.
E-mail address: anoopmukherjee@cgcri.res.in (A.K. Mukhopadhyay).

0272-8842/$34.00
doi:10.1016/j.ceramint.2009.01.002

on Ti6Al4V substrate [8–10]. The reported values on H and E spanned a range of ≈4–5 and 83–123 GPa, respectively as one moved from the coating-substrate interface to the free coating side across the coating cross-section [8]. The nanoindentation data showed further, that Young's modulus value of amorphous zone was much lower than that of the crystalline zone of HAP coating [9,10]. On the other hand, for HAP coating prepared by using an Nd-YAG laser on Ti, the nanoindentation measurements with a Vicker's diamond pyramidal indenter along the coating cross-section showed that both H and E values were lower at the coating side than at the coating-substrate interface [11]. However, depending on processing condition and type of substrates, the magnetron sputtered thin HAP films (350–650 nm) displayed a much higher range of nano-hardness (≈4–9 GPa) and Young's moduli (≈70–150 GPa) when measured with a Berkovich indenter [12,13]. Nano-hardness and Young's moduli data have also been reported for functionally graded coating of HAP/glass composite and HAP/α-TCP composite [14]. Others have evaluated Vicker's microhardness and nano-hardness of various composite coating systems, e.g. (a) plasma sprayed 50 vol.% HAP/50 vol.% Ti6Al4V composite coating on Ti6Al4V substrate [15], (b) plasma sprayed HAP/YSZ/Ti6Al4V composite coating [16], (c) HAP/carbon nanotube (CNT) composite coating [17] and (d) biomimetic HAP coating deposited on Ti6Al4V and Ti13Nb11Zr alloy substrates [18]. Most of these reports involve a Ti6Al4V or Ti or Ti alloy substrate and thus the amount of information on micro- or nano-mechanical properties of microplasma sprayed HAP coating on SS316L substrate is almost insignificantly small. This particular need provided the genesis of the present work.

In general the scatter in data was very high for the plasma sprayed coatings, presumably due to the highly heterogeneous and porous structure of the coatings. To treat this scatter, Weibull statistical analysis has been utilized and the corresponding characteristic values in each case were evaluated to obtain suitable results for structural designing. As a matter of fact, this particular statistical method has been widely utilized to calculate the characteristics values for various mechanical properties of heterogeneous materials; for example to calculate the Young's modulus of the SiC/SiC ceramic matrix composite for turbine vanes [19], the microhardness and Young's modulus of thermal barrier coatings on Ti-alloys [20–22], etc. Thus, the Weibull statistical analysis is a well established, simple and widely used technique to calculate the characteristic properties of such brittle materials with various phases, flaws or defects that results in wide variations in the mechanical properties like hardness and Young's modulus.

From the survey of literature it appears that the local mechanical properties of HAP coating are function of method of preparation of the coating, substrate type, condition of the substrate, coating thickness, test load, loading rate, etc. However, as pointed out above, there has not been any systematic study of local mechanical properties for microplasma sprayed HAP coating on SS316L substrates. Therefore, the objective of the present study was to prepare the HAP coatings on SS316L substrates by microplasma spraying (MPS) technique using a very low plasmatron power (e.g. ∼1.5 kW) and characterize the local mechanical properties, e.g. nano-hardness (H) and Young's modulus (E) of the coatings by the well established nanoindentation technique.

2. Materials and methods

The HAP powder was conventionally synthesized by the usual wet precipitation route. The detail preparation of HAP powder has been described elsewhere [23,24]. The resulting whitish precipitate was subsequently aged, dried, sintered at 1250 °C and sieved to produce sinter-granulated HAP to be used as the starting powder for the microplasma spraying process. Chemical analysis of the powder was performed by inductively coupled plasma–atomic emission spectroscopy (Spectro Flame Modula, Spectro-Analytical Instruments, Model: STM 08, Germany). The size distribution of HAP was measured by a particle size analyzer (Malvern Mastersizer X, Malvern Instruments, Malvern, UK). Flowability of HAP granule was measured as per ASTM B 212-99 standard by a Hall Flowmeter (Lloyds, India).

The substrate used for coating was commercially available surgical grade 316L stainless steel. The substrate was shaped into strips and cylinder of sizes (155 mm × 20 mm × 2 mm) and ($\varphi = 25$ mm, $L = 25.4$ mm), respectively. Flat parallel ground substrate strips were blasted with 200–250 μm alumina grits to roughen the surface to an average roughness (R_a) value of ∼2.5 μm, followed by ultrasonic cleaning (Microclean-109, Oscar Ultrasonics, Mumbai, India) using sequentially AR-grade acetone, ethanol and deionized water.

Thereafter, HAP coatings on SS316L substrates were prepared by the microplasma spraying (MPS) technique at a low plasmatron power of 1.5 kW using a commercial machine (Miller Maxstar 200 SD 2.5 kW). Argon was used as the primary and secondary gases. The MPS-HAP coated SS316L samples were post-heat-treated at 600 °C in air to increase the degree of crystallinity of the coating and the bonding strength.

The phase purity and crystallinity of the MPS-HAP coating on the SS316L were analyzed by X-ray diffraction (Philips PW1710, The Netherlands) using monochromatic Cu Kα1 radiation at 55 mA and 40 kV. The bonding strength of coating was evaluated according to ASTM-C633. The microstructural characterizations and film thickness measurements were carried out by both SEM (scanning electron microscopy, s430i, Leo, UK) and FE-SEM (field emission-scanning electron microscopy, Supra VP35 Carl Zeiss, Germany) and subsequently by an image analyzer (Leica Q500MC, UK). Prior to insertion in the sample chamber for electron microscopy, a 50–70 nm carbon coating was deposited on the HAP coating by the arc deposition technique to avoid charging.

Local mechanical properties, e.g. nano-hardness (H) and Young's modulus (E) were measured on the polished plan section of the HAP coating, i.e. in a direction perpendicular to the splat orientation by the nanoindentation technique using a

commercial machine (Fischerscope H100-XYp; Fischer, Switzerland). The depth sensing resolution and force sensing resolution were 1 nm and 0.2 μN, respectively. The machine was calibrated with nanoindentation based independent evaluation of $H \sim 4.14$ GPa and $E \sim 84.6$ GPa of a Schott BK7 Glass. The experiments were conducted at nine different loads in the range of 10–1000 mN with a Berkovich indenter on the top surface (i.e. plan section) of polished, bonded, 200 μm thick HAP coatings on SS316L substrates. The surface roughness (R_a) of the bonded coating was ~0.5 μm. The maximum depth of penetration was kept within ~5 μm, which is well below 20 μm. The depth of 20 μm was about 10% of the coating thickness. Thus, the measurements were taken from a depth that would avoid the influence of the substrate's mechanical properties on the measured data. The Berkovich indenter had a tip radius of about 150 nm and a semi-apex angle of 65.03°. Both the loading and unloading time were kept at 30 s. At least fifteen indents were made at each load at five different locations of the sample as the nature of the coating was porous and heterogeneous. The nano-hardness (H) and Young's modulus (E) were evaluated according to DIN 50359-1 standard from the load versus depth of penetration plots using the well-established Oliver and Pharr (O–P) model [25].

The scatter in the data was treated in terms of the Weibull statistics analysis. For this purpose, the two-parameter Weibull distribution function was utilized. The function provides the probability, p, for a given parameter, x, as [19,20,22]

$$p = 1 - \exp\left[-\left(\frac{x}{x_o}\right)^m\right] \tag{1}$$

where x_o is known as the scale parameter where the probability of occurrence is 63.2% and "m" is the Weibull modulus. The value of the Weibull modulus is a dimensionless quantity and indicates the degree of scatter in the data. The magnitude of "m" increases with decreasing scatter. The survival probability of the ith observation in the data arranged in ascending order can be expressed as [19,20,22]

$$p = \frac{i - 0.5}{N} \tag{2}$$

where N is the total number of observations. Although, in some literature, the formula for the probability estimator "p" was found to be different, here we have employed the most extensively used expression.

Taking ln for two times of both the sides and simplifying, Eq. (1) can be expressed as

$$\ln\left[\ln\left\{\frac{1}{1-p}\right\}\right] = m[\ln(x) - \ln(x_o)] \tag{3}$$

The values of m and x_o are obtained by fitting the experimental data to Eq. (3), by least square regression. The slope of the straight line will give the value of Weibull modulus (m) and the intercept on the "Y" axis will give the value of scale parameter (x_o). Finally, by setting the value of ln[ln {1/(1 − p)}] equal to zero and placing the values of m and scale-parameter in Eq. (3), one can easily calculate the characteristic value (x_o) of the related parameter, x. The characteristic values (x) are of great engineering importance as it provides the designer with a unique and dependable value of the required parameter. In the present study, x was hardness and Young's modulus. The corresponding characteristic values were termed as H_{char} and E_{char}.

2.1. Basic theory of nanoindentation

During the nanoindentation, the high resolution instrument continuously monitors the load, P and depth of penetration, h of an indenter which in the present investigation was a Berkovich tip. These data are utilized to get the load versus depth of penetration ($P - h$) data plot. The important physical quantities obtained from the load versus depth of penetration plot are: the peak load, P_{max}, maximum penetration depth, h_{max}, final penetration depth, h_f, and the contact stiffness, S.

According to the O–P model [25] which is the most commonly used method to obtain the hardness and Young's modulus of a material by instrumented nanoindentation, the nano-hardness (H) is expressed as

$$H = \frac{P_{max}}{A_{cr}} \tag{4}$$

where P_{max} is the maximum applied load and A_{cr} is the real contact area between the indenter and the material. According to Oliver and Pharr, the polynomial form of A_{cr} can be expressed as [26]

$$A_{cr} = 24.56h_c^2 + C_1h_c + C_2h_c^{1/2} + C_3h_c^{1/4} + \cdots + C_8h_c^{1/128} \tag{5}$$

where C_1–C_8 are constants to be determined by standard calibration method and h_c is the penetration depth determined from the following expression [26]:

$$h_c = h_{max} - \kappa\left(\frac{P_{max}}{S}\right) \tag{6}$$

where $\kappa \approx 0.75$ for a Berkovich indenter [27].

Again, the contact stiffness (S) which is the slope of the first ~1/3rd linear part recorded during the unloading cycle of the load versus depth of penetration plot can be expressed as [28]

$$S = \left(\frac{dP}{dh}\right)_{h=h_{max}} = \alpha C_A E^* \sqrt{A_{cr}} \tag{7}$$

where $\alpha = 1.034$ and $C_A = 2/\sqrt{\pi}$ for a Berkovich indenter [28] and E^* is the effective Young's modulus. Following the O–P model, E^* can be expressed as [25]

$$\frac{1}{E*} = \frac{(1-\nu_i^2)}{E_i} + \frac{(1-\nu_s^2)}{E_s} \tag{8}$$

where E and ν are the Young's modulus and Poisson's ratio, respectively and subscripts i and s, denotes the indenter and the sample, respectively. For the Berkovich diamond indenter used in the present work, the values of E_i and ν_i were taken as 1140 GPa and 0.07 respectively, following [28].

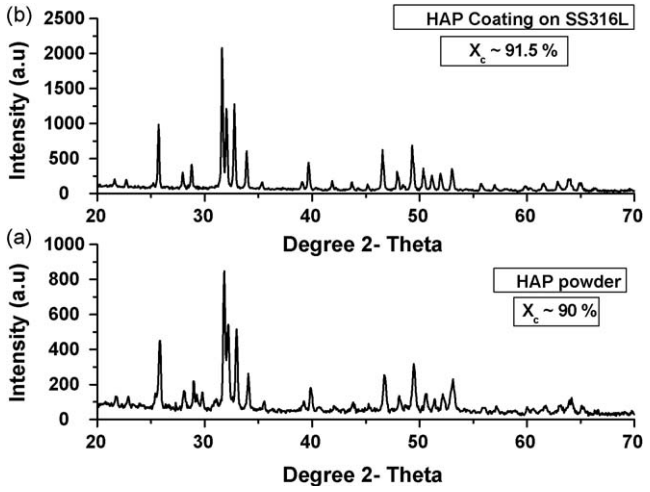

Fig. 1. X-ray diffraction pattern of: (a) synthesized HAP powder and (b) MPS-HAP coating on SS316L.

3. Results and discussion

In the present work, the Ca/P ratio of HAP powder was maintained at ~1.67. The mean HAP granule size (d_{50}) was ~67 μm. The X-ray diffraction (XRD) patterns of both the HAP powder and the MPS-HAP coating on SS316L are shown in Fig. 1(a) and (b). The XRD of HAP powder showed the presence of only HAP peaks (JCPDS file no: 09-0432) confirming it to be a single-phase material (Fig. 1(a)). In the coated samples also no peaks other than HAP was observed indicating no change in phase composition during coating. The degree of crystallinity (X_c) calculated following [29] was ~90% and ~91% for the HAP powder and HAP coating, respectively. The surface morphology of as sprayed and polished top surface, i.e. plan section of the coating is shown through scanning electron micrographs in Fig. 2(a) and (b), respectively. Both the splat size and the vol.% open porosity were measured by an image analyzer taking several FE-SEM images with same magnification from different areas of the as sprayed (Fig. 2(a)) and the polished plan section (Fig. 2(b)) of the MPS-HAP coating on SS316L substrate. The splat size of the coating was ~50–70 μm. The macro-pore size and micro-pore size of the coating were ~10–30 μm and ~1 μm, respectively. The average vol.% open porosity was ~18%. The bonding strength of the MPS-HAP coating measured according to the ASTM-633-01 standard was found to be ~13 MPa.

3.1. Nano-hardness and Young's modulus

The well known O–P model [25] was utilized in the present work to calculate the micromechanical properties of the plan section of the ~200 μm thick MPS-HAP coating at nine different loads in the range of 10–1000 mN. However, the results obtained from the O–P model [25] will be erroneous if the area function used to calculate the contact area ($A_{cr,}$ Eq. (5)) in this model gets modified [28]. Thus, to verify the applicability of this model, it is always necessary to calculate the (h_f/h_{max}) ratio from the load versus depth of penetration

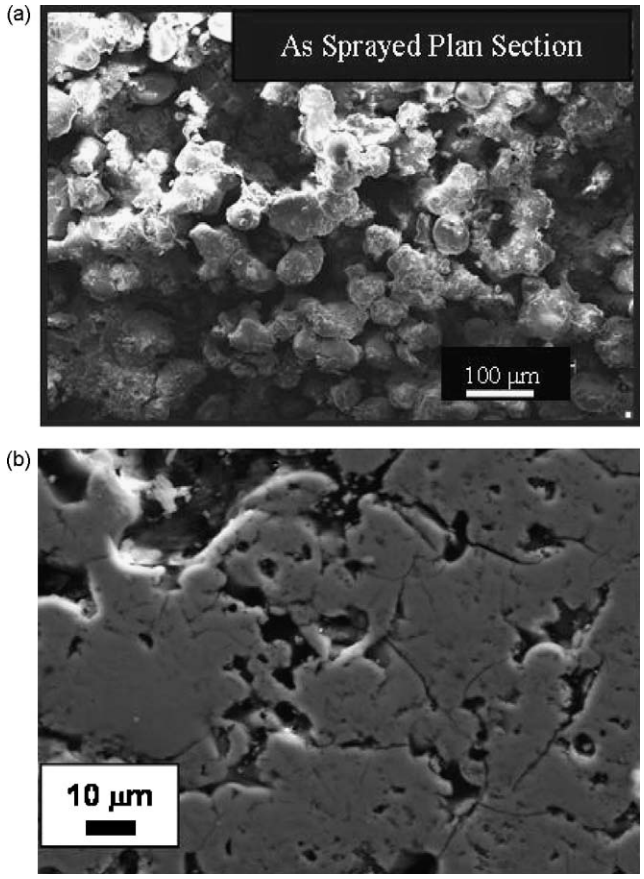

Fig. 2. Photomicrograph of MPS-HAP coating: (a) plan section in as-sprayed condition taken in a scanning electron microscope and (b) polished plan section taken in a field emission scanning electron microscope (FE-SEM).

plot. The value of this ratio should lie below 0.7 to obtain reliable results from the O–P model [28,30]. The average values of (h_f/h_{max}) ratio for the coating in the present study were below 0.7 (Fig. 3). This information justified the basic applicability of the O–P model to analyze the nanoindentation data of the present MPS-HAP coatings on SS316L.

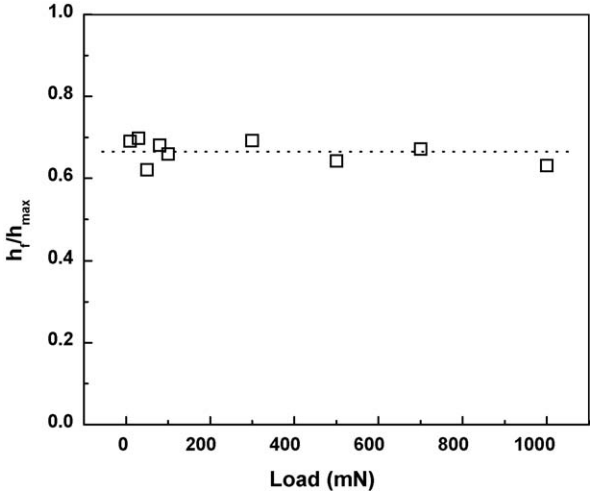

Fig. 3. The ratio of h_f/h_{max} for HAP coating under 10–1000 mN loading condition.

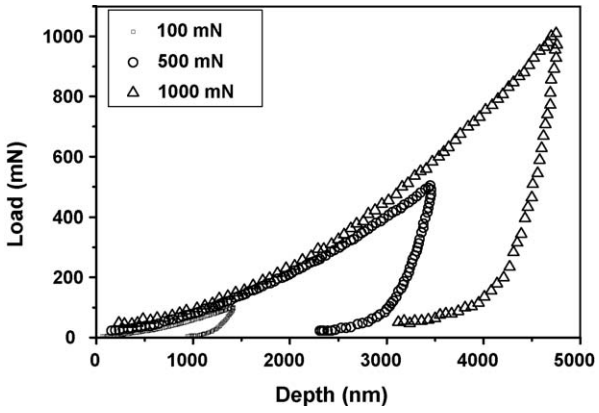

Fig. 4. The load–depth ($P - h$) plots of MPS-HAP coating at low load (100 mN) and high loads (e.g. 500 and 1000 mN).

The typical average load–depth ($P - h$) plots at low load (100 mN) and high loads (500 and 1000 mN) with a Berkovich indenter are shown in Fig. 4. At higher indentation loads as expected there was a large residual depth, e.g. about 3000 nm and consequently, a larger area encompassed by the load versus depth plot implying dissipation of higher amount of energy as compared to those involved at lower or intermediate loads. SEM image of a single Berkovich at low load, e.g. 80 mN load is shown in Fig. 5. The indentation area looked smooth without any imminent sign of severe damage growth or accumulation.

The Weibull distribution fitting was done for the nano-hardness (H) and Young's modulus (E) of the coating, as determined by the nanoindentation experiment. The Weibull distribution fittings for H and E data are shown in Figs. 6 and 7. The variation of the Weibull modulus with load for both nano-hardness and Young's modulus data are shown in Fig. 8(a) and (b), respectively.

At low load, the scatter was high, so the Weibull modulus had a low value, e.g. "m" = 2.72 for nano-hardness data (Fig. 6) and "m" = 4.59 for Young's modulus data (Fig. 7) obtained at 30 mN. The reason for high scatter was that the coating was full of surface defects like macro-pores, micro-pores, intra-splat

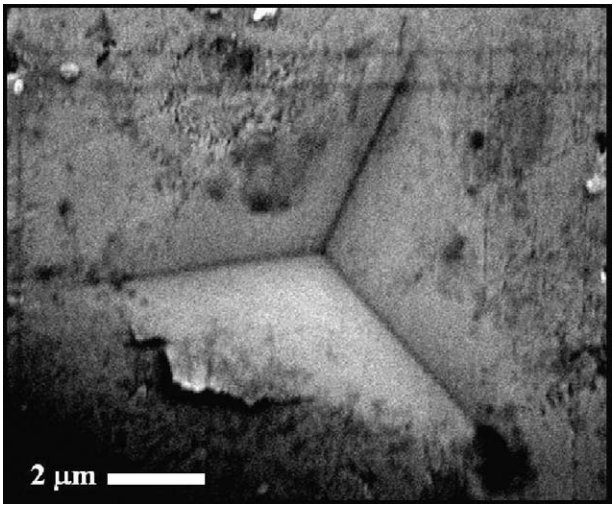

Fig. 5. SEM image of a single Berkovich indent at 80 mN load.

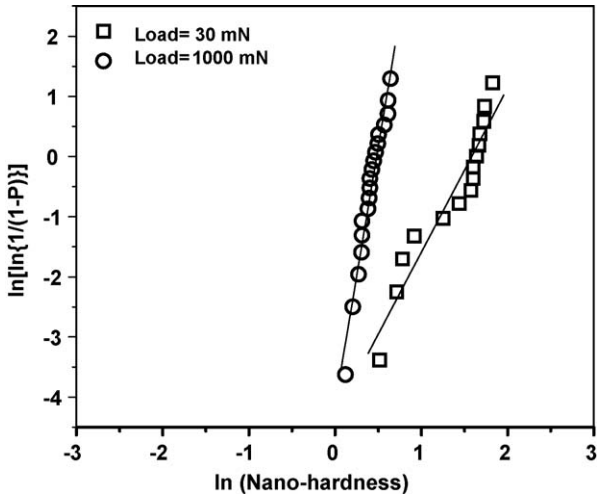

Fig. 6. Weibull distribution fittings of nano-hardness (H) data on the plan section of MPS-HAP coating at 30 and 1000 mN load.

cracks and inter-splat cracks and also many shallow cracks and defects lying in very close vicinity of the sub-surface region. These flaws would have a statistical size distribution due to the process of plasma spraying. At low load, the depth of penetration was small and therefore, the indentation zone of influence was also small. As the indentation size/depth scales with the size of such flaws as mentioned above, the scatter of data was relatively higher, as revealed from the plots of data in Figs. 6 and 7.

The scenario reverts completely at a higher load of indentation. At high load, the scatter was relatively lower, so the Weibull modulus had a high value, e.g. "m" = 8.58 for nano-hardness data (Fig. 6) and "m" = 17.05 for Young's modulus data (Fig. 7) obtained at 1000 mN. The scatter was low because the uncertainty of measured data decreased with increase of indentation load; Fig. 8(a) and (b). Similar observations have been made by others [31,32]. Physically, at a higher load of indentation, the depth of penetration was more and as a result the indentation zone of influence was

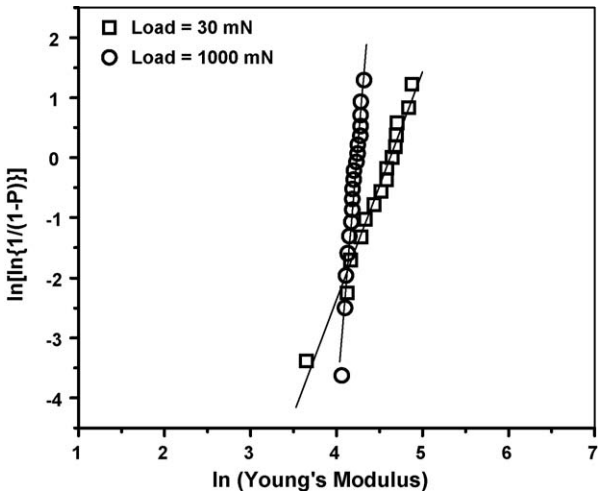

Fig. 7. Weibull distribution fittings of Young's modulus (E) data on the plan section of MPS-HAP coating at 30 and 1000 mN load.

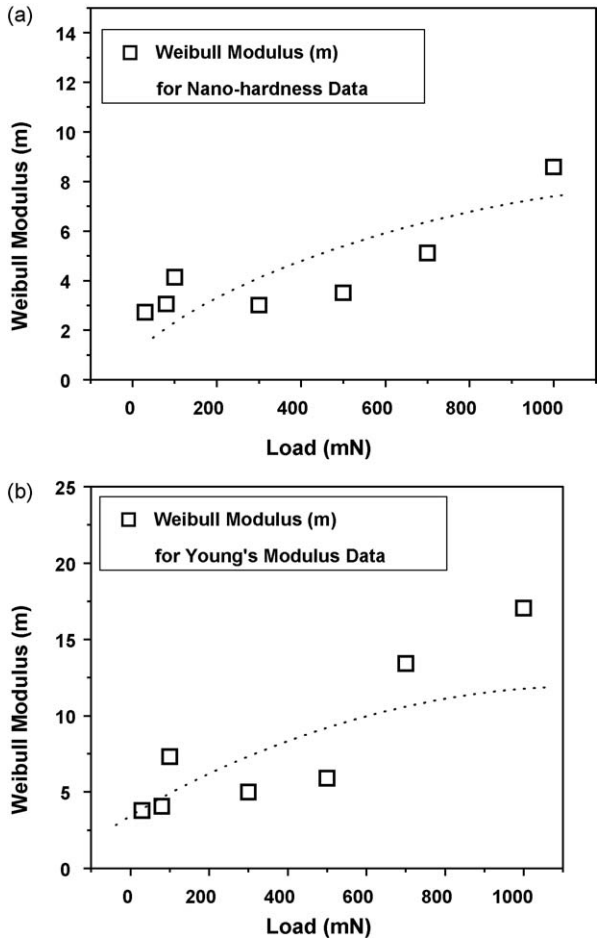

Fig. 8. Weibull modulus (m) values of MPS-HAP coating as a function of load for: (a) nano-hardness and (b) Young's modulus.

having a larger volume compared to those obtained at a lower load of indentation. In such a larger zone of influence, the possibilities are high that many interactions between the penetrating indenter and a large variety of deep cracks, pores and other defects with a large variety of random local spatial orientation would take place and in the process would ultimately result in an averaging effect in such a fashion that the overall scatter could reflect a decreasing trend. A strong support for this conjecture, in fact, was borne out from the Weibull moduli data of nano-hardness and Young's moduli of the MPS-HAP coating, plotted as a function of load in Fig. 8(a) and (b), wherein both the data showed an overall average trend of increasing with load.

Thus, our experimental data would suggest that the extent of scatter in the nano-hardness and Young's modulus data measured by nanoindentation at low load was governed in the present MPS-HAP coating by the presence of very shallow surface and sub-surface defects. However, those measured at relatively higher load of nanoindentation might be governed not only by the statistical distribution of larger pores and deeper crack-like defects but also by differences in their local orientation which might have been conducive enough to provide ultimately an averaging out effect, to reduce the overall range of the data being evaluated.

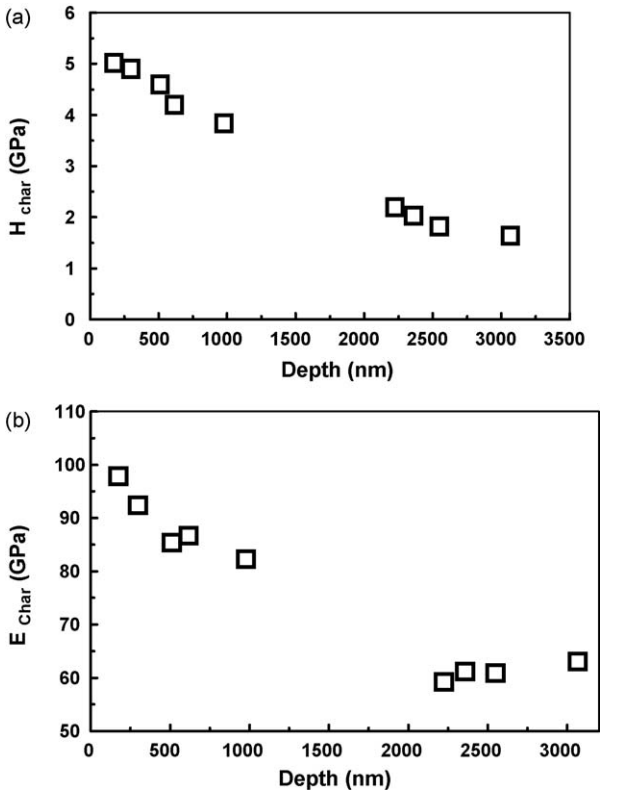

Fig. 9. Influence of penetration depth on: (a) nano-hardness (H) and (b) Young's modulus (E) of the plan section of MPS-HAP coating.

Further, the characteristic values of H (H_{char}) and E (E_{char}) were obtained for each load. These values were plotted as a function of load (Fig. 9(a) and (b)). At a low load of 10 mN, the coating showed H_{char} value ~5 GPa at a depth of about 200 nm which dropped by about 60%, e.g. ~2 GPa at a depth of ~3000 nm for a higher load of 1000 mN ((Fig. 9(a)). Thus, a strong indentation size effect (ISE) was present in the data. The corresponding E_{char} values were about 100 and 60 GPa (Fig. 9(b)) at 10 and 1000 mN loads, respectively. Although a direct comparison of the data of present work with literature data was not possible because the processing method and measurement methods were not all identical, still it may be mentioned that the data of the present work compared favourably with the literature data [8–10,12,13]. However, the data reported [11] for laser deposited HAP coating was slightly higher than those measured in the present work.

The nano-hardness and Young's modulus value of sintered bulk HAP were reported as 6 and 125 GPa, respectively [14]. The nano-hardness and Young's modulus of the plasma sprayed coatings as measured in the present work (average $H \sim 3.5$ GPa, average $E \sim 80$ GPa) were much reduced compared to that of the bulk sintered HAP material. This was due to the fact that the coating had a high porosity of about 18 vol.%. A high density of planner and volumetric crack-like defects with very little preferred orientation were shown in Fig. 2(b). Work done on plasma sprayed ceramic thermal barrier coatings has already established that volumetric and planner defects could cause significant reduction of both hardness and Young's modulus values [33,34].

The dependence of Young's modulus (E) on vol.% porosity (p) is expressed as [35]

$$E = E_0 \exp(-b\,p) \tag{9}$$

where b is a constant (~2.5), E_0 is the Young's modulus for a material with zero porosity, i.e. of theoretical density. Assuming $E_0 = 125$ GPa [14], for a HAP coating with 18 vol.% porosity, the predicted Young's modulus value was ~79 GPa, which matched quite well with the load averaged Young's modulus data of 80 GPa as mentioned above. The reduced hardness value was calculated as ~3.8 GPa by the similar relation adapted for the hardness vs. porosity, assuming H_0 as 6 GPa [14]. This also matched well with the load averaged hardness data of 3.5 GPa. Further, it may be noted also that the load averaged values of characteristic Young's modulus (E_{char}) and hardness (H_{char}) were calculated as 76.53 and 3.34 GPa, respectively. These values were also well matched with the predicted value of hardness and Young's modulus.

The nano-hardness obtained from the geometrically similar indenters, i.e. conical or pyramidal (e.g. Knoop, Vickers, Berkovich, etc.) at various loads is in principle expected to remain unchanged as the strain during the indentation is constant unlike the spherical indenter. However, in a practical situation, the hardness using similar indentations is found to vary with the load. The increase in hardness with decreasing load, which is known as indentation size effect, is often observed in bulk ceramics [36–39], physically and chemically vapour deposited ceramic coatings [40,41] as well as in plasma sprayed ceramic coatings [21,31,42,43]. In the present work, ISE also was observed (Fig. 9(a)).

The most widely used empirical equation for describing the ISE is the Meyer's law. This law correlates the test load and the resultant indentation size using a simple power law [37,44–47]

$$P_{max} = A_1 h_c^n \tag{10}$$

where A_1 and n are constants that can be derived directly from the experimental data by any suitable regression technique. When the value of "n" lies between 1 and 2; it can be attributed to the definite presence of an ISE.

Through linear regression analysis, the best-fit values of the parameters A_1 and n were obtained as 5.3×10^{-4} mN/nm^n and 1.48, respectively (Fig. 10). The high value of the correlation coefficient, r (e.g. $r = 0.99$) implied that Eq. (10) could provide a satisfactory description of the nanoindentation data of present work. Since the value of "n" lies between 1 and 2, it can be attributed to the definite presence of an ISE in the data.

An alternative approach to the explanation of the ISE phenomenon has been put forward by Hays and Kendall [48]. It has been proposed that the basis of the ISE is the existence of a minimum level of the indentation test load, W_i, below which permanent deformation or flow does not initiate, but only elastic deformation occurs. So, philosophically one can associate W_i with a basic, minimum intrinsic force that exist

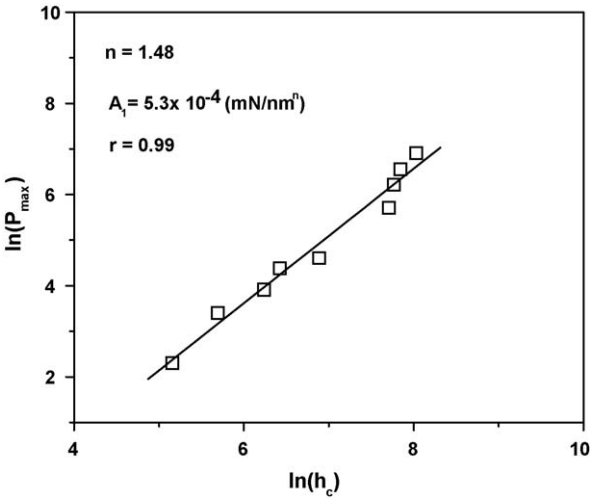

Fig. 10. Dependency of $\ln(P_{max})$ on $\ln(h_c)$ according to the Meyer's law.

at the specimen surface. We prefer to call this term as sample resistance ($W_i = R$).

To explain ISE in the case of nanoindentation data taken with a Berkovich indenter for glass as well as bulk TZP and silicon nitride ceramics, the following equation has been proposed [49]

$$P_{eff} = P_{max} - R = A_2 h_c^2 \tag{11}$$

where P_{eff} represents the effective load that is available for doing the actual work of indentation after passing over the specimen's intrinsic resistance (R), P_{max} is the applied maximum load and A_2 is a constant. At lower applied loads the effective load is quite low, and the corresponding indentation depth is very small. This in turn results in a higher hardness value. This effect gradually diminishes with the increase in load, thus producing the indentation size effect as observed in the present work. A linear regression analysis of P_{max} vs. h_c^2 has been carried out and from the intercepts of the best fitted line (Fig. 11), the value of $R = 2.38$ mN was evaluated for the present MPS HAP samples. Similarly the value of A_2 was estimated as 0.98×10^{-4} mN/nm^2. Thus, for an applied load of

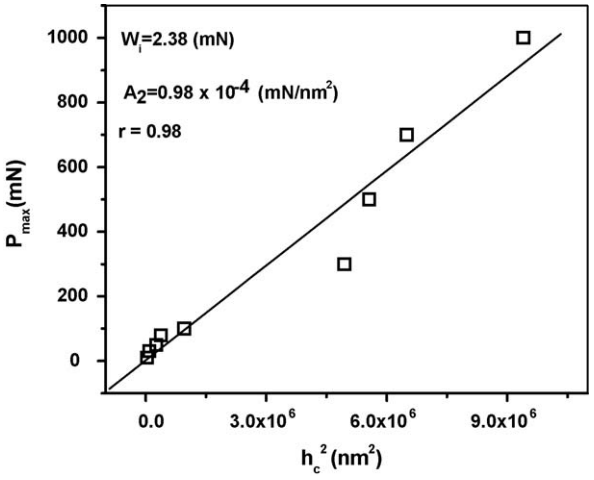

Fig. 11. Dependency of P_{max} on h_c^2 according to the Hays–Kendall approach.

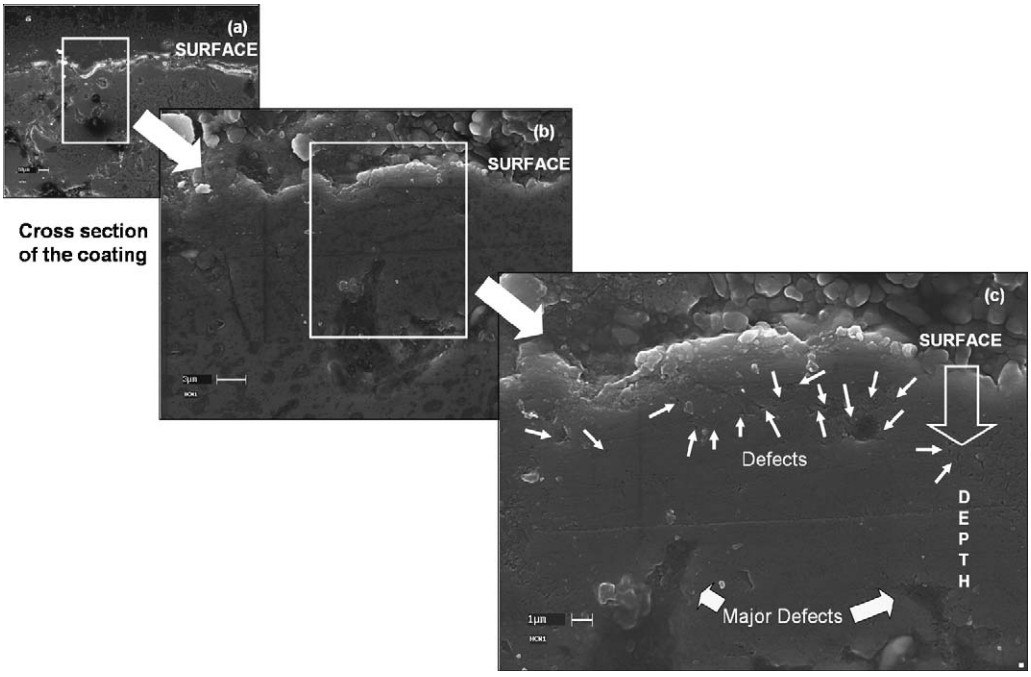

Fig. 12. SEM photomicrographs of the polished cross-section of the MPS-HAP coating taken at progressively higher magnifications: (a) at ×1K; (b) ×6K; (c) ×10K.

10 mN, the effective load available for carrying out the work of indentation was about 7.62 mN. For such an effective load, from Eq. (11), we can then estimate h_c as 0.278 μm and the corresponding nano-hardness as about 5.23 GPa. Both of these data matched reasonably well with the experimentally measured data of depth (h_c) ∼0.29 μm and nano-hardness ∼5.02 GPa. The small value of sample resistance, R indicates that this approach can explain the ISE phenomenon successfully. Furthermore, the high correlation coefficient ($r \sim 0.98$) implied that Eq. (11) provides a satisfactory description of the nanoindentation data for the MPS-HAP materials.

Indentation size effect as encountered in both metallic [50] and brittle [51] materials, is a significant phenomenon in micro- and nanoindentation tests describing the increase in hardness values with decrease of the indentation loads. In the past few decades, a number of explanations have been developed for ISE, including: the well established strain gradient plasticity theory [52], dislocation nucleation [53]; variation of contact surface [54]; friction between the surface and the indenter [55] and the micro-fracture processes [56].

However, in our case SEM evidences taken from the coating cross-section at progressively higher magnification showed that there was a gradual increase of fine micro-pores and micro-cracks as well as macroscopic defects such as large macro-pores and deeper cracks as one traverses from the surface towards the depth of the coating (Fig. 12(a)–(c)). When the penetrating indenter traverses a larger depth in the MPS-HAP coating at a higher indentation load (e.g. about 3060 nm at a load of 1000 mN), it is most likely to come across a large sub-surface macro-pore or crack, which would cause an apparent increase in depth of penetration and thereby affect a larger area of contact, which, in turn would be reflected in a lower nano-hardness value being evaluated.

On the contrary, at very low load of indentation, e.g. at 10 mN, the depth of penetration was indeed very much shallow at about 170 nm which contributed to a lower area of contact. In case the area of contact is lower, the hardness being evaluated would be on the higher side, as, in fact, has been reflected in our data (Fig. 9(a)). Therefore, based on our experimental data and the scanning electron microscopy based observations we suggest that the extent of interaction of the indenter with average size defects across the depth of a microplasma sprayed HAP coating may cause an indentation size effect.

The presence of fine pores and micro-cracks at different depths from surface would make the MPS-HAP coating more compliant to deformation. As a result, at a given load the indenter would penetrate to higher depth in the presence of such pores and cracks than that it could have in their absence [57]. Higher depth of penetration would result in a larger area of contact and hence a lower hardness. Conversely, at lower loads of indentation, the depth of penetration has smaller magnitude. In other words they remain very close (e.g. at about 200 nm) to the surface. Thus, the nanoindent itself would then have much lesser chance to interact with intrinsic defects which lie at a much higher depth (e.g. at least 500 nm or greater, Fig. 9(a)). As a result, the lower depth of penetration would result in a smaller area of contact and hence a much higher hardness, thus possibly producing the indentation size effect as observed in the present work.

4. Summary and conclusions

Phase pure and flowable HAP granule was prepared from the conventional wet chemical route. HAP coatings of thickness ∼200 μm were prepared by microplasma spraying on SS316L substrates. The degree of crystallinity for MPS-HAP was found

to be high (∼91%). Nanoindentation study was conducted to evaluate local mechanical properties. The statistical validity of the data was established through the application of Weibull statistics, because of the porous and heterogeneous nature of the coating. The "*m*" value for the nano-hardness (*H*) varied in the range 2–9. For the Young's modulus (*E*), the "*m*" value varied in the range of 3–18. For both *H* and *E* values of the coating, the values of the Weibull modulus ("*m*") showed an overall increasing trend with respect to load although there were some occasional deviations. Such deviations might have occurred due to the presence of pores and cracks in different layers of the coating. It was postulated that higher scatter of data at lower load could be linked to stochastic nature of interaction between the indenter that penetrated a very shallow depth and the flaws that scale with the size/depth of the indentation and which possessed a highly statistical size distribution in the surface and in the close vicinity of sub-surface region. At higher load, it was suggested that due to a larger indentation zone of influence, an averaging out effect of indenter-flaw interaction predominated to affect a reduction in data scatter. At a low load of 10 mN, the coating showed a hardness value of about 5 GPa at a depth of about 170 nm which dropped by 60%, e.g. ∼2 GPa at a depth of about 3000 nm for a higher load of 1000 mN. These data suggested the presence of a strong indentation size effect in the nano-hardness behaviour of the coatings. The corresponding Young's moduli data were about 100 and 60 GPa at 10 and 1000 mN loads, respectively. Based on our experimental data and the scanning electron microscopy based observations it has been suggested that the extent of interaction of the indenter with average size defects across the depth of a microplasma sprayed HAP coating could be responsible for the observed indentation size effect.

Acknowledgements

The authors are grateful to Director, Central Glass and Ceramic Research Institute (CGCRI), Kolkata for his kind permission to publish this paper and to Dr. D.K. Bhattacharya, Head, Analytical Facility Division of CGCRI for his kind encouragements during the course of this work. Finally, the authors appreciate the infrastructural support received from all colleagues and particularly that received from the colleagues of the Mechanical Test Section and Bio-Ceramics and Coating Division at CGCRI. Finally, the authors gratefully acknowledge financial support received from DST-SERC (Project No: GAP 0216) and CSIR (Network Project TAREMAC No: NWP 0027).

References

[1] L.L. Hench, Bioceramics, J. Am. Ceram. Soc. 81 (1998) 1705–1728.
[2] R.S. Lima, K.A. Khor, H. Li, P. Cheang, B.R. Marple, HVOF spraying of nanostructured hydroxyapatite for biomedical applications, Mater. Sci. Eng. A 396 (2005) 181–187.
[3] W. Tong, J. Chen, X. Li, Y. Cao, Z. Yang, J. Feng, X. Zhang, Effect of particle size on molten states of starting powder and degradation of the relevant plasma-sprayed hydroxyapatite coatings, Biomaterials 17 (1996) 1507–1513.
[4] L. Zhao, K. Bobzin, F. Ernst, J. Zwick, E. Lugscheider, Study on the influence of plasma spray processes and spray parameters on the structure and crystallinity of hydroxylapatite coatings, Mat. Wiss. u. Werkstofftech. 37 (2006) 516–520.
[5] G. Rondelli, B. Vicentini, A. Cigada, Localized corrosion tests on austenitic stainless steels for biomedical applications, Br. Corr. J. 32 (1997) 193–196.
[6] T.M. Sridhar, U.K. Mudali, M. Subbaiyan, Sintering atmosphere and temperature effects on hydroxyapatite coated type 316L stainless steel, Corr. Sci. 45 (2003) 2337–2359.
[7] T.M. Sridhar, U.K. Mudali, M. Subbaiyan, Preparation and characterisation of electrophoretically deposited hydroxyapatite coatings on type 316L stainless steel, Corr. Sci. 45 (2003) 237–252.
[8] K.A. Khor, H. Li, P. Cheang, Characterization of the bone-like apatite precipitated on high velocity oxy-fuel (HVOF) sprayed calcium phosphate deposits, Biomaterials 24 (2003) 769–775.
[9] C. Zhang, Y. Leng, J. Chen, Elastic and plastic behavior of plasma-sprayed hydroxyapatite coatings on a Ti–6Al–4V substrate, Biomaterials 22 (2001) 1357–1363.
[10] J. Wen, Y. Leng, J. Chen, C. Zhang, Chemical gradient in plasma-sprayed HA coatings, Biomaterials 21 (2000) 1339–1343.
[11] G.J. Cheng, D. Pirzada, M. Cai, P. Mohanty, A. Bandyopadhyay, Bioceramic coating of hydroxyapatite on titanium substrate with Nd-YAG laser, Mater. Sci. Eng. C 25 (2005) 541–547.
[12] T.G. Nieh, A.F. Jankowski, J. Koike, Processing and characterization of hydroxyapatite coatings on titanium produced by magnetron sputtering, J. Mater. Res. 16 (2001) 3238–3245.
[13] T.G. Nieh, B.W. Choi, A.F. Jankowski, Synthesis and characterization of porous hydroxyapatite and hydroxyapatite coatings, in: Proceedings of the Minerals, Metals, and Materials Society Annual Meeting & Exhibition, New Orleans, LA, February 11–15., 2001.
[14] R.R. Kumar, M. Wang, Modulus and hardness evaluations of sintered bioceramic powders and functionally graded bioactive composites by nano-indentation technique, Mater. Sci. Eng. A 338 (2002) 230–236.
[15] Y.W. Gu, K.A. Khor, P. Cheang, In vitro studies of plasma-sprayed hydroxyapatite/Ti-6Al-4V composite coatings in simulated body fluid (SBF), Biomaterials 24 (2003) 1603–1611.
[16] K.A. Khor, Y.W. Gu, D. Pan, P. Cheang, Microstructure and mechanical properties of plasma sprayed HA/YSZ/Ti–6Al–4V composite coatings, Biomaterials 25 (2004) 4009–4017.
[17] Y. Chen, Y.Q. Zhang, T.H. Zhang, C.H. Gan, C.Y. Zheng, G. Yu, Carbon nanotube reinforced hydroxyapatite composite coatings produced through laser surface alloying, Carbon 44 (2006) 37–45.
[18] A. Bigi, M. Fini, B. Bracci, E. Boanini, P. Torricelli, G. Giavaresi, N.N. Aldini, A. Facchini, F. Sbaiz, R. Giardino, The response of bone to nanocrystalline hydroxyapatite-coated Ti13Nb11Zr alloy in an animal model, Biomaterials 29 (2008) 1730–1736.
[19] P.L.N. Murthy, N.N. Nemeth, D.N. Brewer, S. Mital, Probabilistic analysis of a SiC/SiC ceramic matrix composite turbine vane, Comp. Part B: Eng. 39 (2008) 694–703.
[20] H. Zhou, F. Li, B. He, J. Wang, B. Sun, Air plasma sprayed thermal barrier coatings on titanium alloy substrates, Surf. Coat. Technol. 201 (2007) 7360–7367.
[21] D. Basu, C. Funke, R.W. Steinbrech, Effect of heat treatment on elastic properties of separated thermal barrier coatings, J. Mater. Res. 14 (1999) 4643–4650.
[22] S. Guo, Y. Kagawa, Effect of thermal exposure on hardness and Young's modulus of EB-PVD yttria-partially-stabilized zirconia thermal barrier coatings, Ceram. Int. 32 (2006) 263–270.
[23] M.K. Sinha, D. Basu, P.S. Sen, Porous hydroxyapatite ceramics and its clinical applications, Interceramics 2 (2000) 102–105.
[24] B. Kundu, M.K. Sinha, M.K. Mitra, D. Basu, Fabrication and characterization of porous hydroxyapatite ocular implant followed by an in vivo study in dogs, Bull. Mater. Sci. 27 (2004) 133–140.
[25] W.C. Oliver, G.M. Pharr, An improved technique for determining hardness and elastic modulus using load and displacement sensing indentation experiments, J. Mater. Res. 7 (1992) 1564–1583.
[26] Z. Ling, J. Hou, A nanoindentation analysis of the effects of microstructure on elastic properties of Al_2O_3/SiC composites, Comput. Sci. Techol. 67 (2007) 3121–3129.

[27] D. Zhu, D. Hongna, F. Luo, W. Zhou, Preparation and mechanical properties of C/C–SiC composites, Mater. Sci. Forum 546–549 (2007) 1501–1504.
[28] S. Guicciardi, A. Balbo, D. Sciti, C. Melandri, G. Pezzotti, Nanoindentation characterization of SiC-based ceramics, J. Eur. Ceram. Soc. 27 (2007) 1399–1404.
[29] M.B. Conz, J.M. Granjeiro, G.A. Soares, Physicochemical characterization of six commercial hydroxyapatites for medical-dental applications as bone graft, J. Appl. Oral Sci. 13 (2005) 136–140.
[30] A. Bolshakov, G.M. Pharr, Influences of pile-up on the measurement of mechanical properties by load and depth sensing indentation techniques, J. Mater. Res. 13 (1998) 1049–1058.
[31] J. Malzbender, R.W. Steinbrech, Determination of the stress-dependent stiffness of plasma-sprayed thermal barrier coatings using depth-sensitive indentation, J. Mater. Res. 18 (2003) 1975–1984.
[32] H. Meinhard, P. Grau, Hardness measurement on rough surfaces, Härterei-Technische Mitteilungen 56 (2001) 287–293.
[33] J.S. Wallace, J. Llavsky, Elastic modulus measurements in plasma sprayed deposits, J. Therm. Spray Technol. 7 (1998) 521–526.
[34] S. Guo, Y. Kagawa, Young's moduli of zirconia top-coat and thermally grown oxide in a plasma-sprayed thermal barrier coating system, Scr. Mater. 50 (2004) 1401–1406.
[35] R.W. Rice, Microstructure dependence of mechanical behaviour of ceramics, in: R.C. MaCrone (Ed.), Treatise on Materials Science and Technology II, Academic Press, New York, 1977, p. 200.
[36] J. Gong, Z. Guan, Effect of microcracking on the energy–balance relationship for hardness testing of ceramics, Mater. Lett. 49 (2001) 180–184.
[37] J. Gong, J. Wu, Z. Guan, Examination of the indentation size effect in low-load Vickers hardness testing of ceramics, J. Eur. Ceram. Soc. 19 (1999) 2625–2631.
[38] S. Guicciardi, D. Sciti, M. Cesare, A. Bellosi, Nanoindentation characterization of submicro and nano sized liquid phase sintered SiC ceramics, J. Am. Ceram. Soc. 87 (2004) 2101–2107.
[39] G. Feng, W.D. Nix, Indentation size effect in MgO, Scr. Mater. 51 (2004) 599–603.
[40] F. Attar, Hardness evaluation of thin ceramic coatings on tool steel, Surf. Coat. Technol. 78 (1996) 78–86.
[41] R.G. Wellman, A. Dyer, J.R. Nicholls, Nano and micro indentation studies of bulk zirconia and EB PVD TBCs, Surf. Coat. Technol. 176 (2004) 253–260.
[42] W. Feng, D. Yan, J. He, G. Zhang, G. Chen, W. Gu, S. Yang, Microhardness and toughness of the TiN coating prepared by reactive plasma spraying, Appl. Surf. Sci. 243 (2005) 204–213.
[43] S. Ghosh, S. Das, T.K. Bandyopadhyay, P.P. Bandyopadhyay, A.B. Chattopadhyay, Indentation responses of plasma sprayed ceramic coatings, J. Mater. Sci. 38 (2003) 1565–1572.
[44] G.N. Babini, A. Bellosi, C. Galassi, Characterization of hot-pressed silicon nitride-based materials by microhardness measurements, J. Mater. Sci. 22 (1987) 1687–1693.
[45] A.K. Mukhopadhyay, S.K. Datta, D. Chakraborty, On the microhardness of silicon nitride and sialon ceramics, J. Eur. Ceram. Soc. 6 (1990) 303–311.
[46] H. Li, R.C. Bradt, The microhardness indentation load/size effect in rutile and cassiterite single crystals, J. Mater. Sci. 28 (1993) 917–926.
[47] K.l. Sangwal, B. Surowska, P. Blaziak, Analysis of the indentation size effect in the microhardness measurement of some cobalt-based alloys, Mater. Chem. Phys. 77 (2003) 511–520.
[48] C. Hays, E.G. Kendall, An analysis of Knoop microhardness, Metallics 6 (1973) 275–282.
[49] Z. Peng, J. Gong, H. Miao, On the description of indentation size effect in hardness testing for ceramics: analysis of the nanoindentation data, J. Eur. Ceram. Soc. 24 (2004) 2193–2201.
[50] Q. Ma, D.R. Clarke, Size dependence of the hardness of silver single crystals, J. Mater. Res. 10 (1995) 853–863.
[51] S.J. Bull, T.F. Page, E.H. Yoffe, An explanation for the indentation size effect in ceramics, Phil. Mag. Lett. 59 (1989) 281–288.
[52] W.D. Nix, H. Gao, Indentation size effects in crystalline materials: a law for strain gradient plasticity, J. Mech. Phys. Solid 46 (1998) 411–425.
[53] M.F. Horstemeyer, M.I. Baskes, S.J. Plimpton, Length scale and time scale effects on the plastic flow of fcc metals, Acta Mater. 49 (2001) 4363–4374.
[54] A. Iost, R. Bigot, Indentation size effect: reality or artifact? J. Mater. Sci. 31 (1996) 3573–3577.
[55] H. Li, A. Gosh, Y.H. Han, R.C. Bradt, The frictional component of the indentation size effect in low load microhardness testing, J. Mater. Res. 8 (1993) 1028–1032.
[56] M.V. Swain, M. Wittling, Fracture Mechanics of Ceramics, Plenum Press, New York, 1996.
[57] K. Duan, R.W. Steinbrech, Influence of sample deformation and porosity on mechanical properties by instrumented microindentation technique, J. Eur. Ceram. Soc. 18 (1998) 87–93.